ISSN 1726-5749

SENSORS & TRANSDUCERS

8 /09
vol. 6
Special

Modern Sensing Technologies II

International Frequency Sensor Association Publishing

IFSA

Sensors & Transducers

Volume 6, Special Issue
August 2009

www.sensorsportal.com

ISSN 1726-5479

Sensors & Transducers Journal (ISSN 1726-5479) is a peer review international journal published monthly online by International Frequency Sensor Association (IFSA).
Available in electronic and on CD.

Sensors & Transducers Journal

Contents

Volume 6
Special Issue
August 2009

www.sensorsportal.com

ISSN 1726-5479

Research Articles

Sensors & Transducers Journal, Vol. 6, Special Issue, August 2009, pp. 128-145

Sensors & Transducers
ISSN 1726-5479

http://www.sensorsportal.com

Compensation of Imperfections for Vibratory Gyroscope Systems Using State Observers

Chien-Yu CHI and *Tsung-Lin CHEN
Department of Mechanical Engineering, National Chiao Tung University,
Hsinchu, Taiwan 30056, R.O.C.
*Tel.: +886-3-571-2121 #55127, fax: +886-3-572-0634
*E-mail: tsunglin@mail.nctu.edu.tw

Received: 10 July 2009 /Accepted: 31 July 2009 /Published: 10 August 2009

Abstract: This paper presents a novel approach that can compensate errors resulting from the imperfections of mechanical structures and interface circuits for MEMS gyroscope systems. Different from most of existing researches on gyroscopes wherein the mechanical structure and interface circuit are either assumed to be ideal or optimized individually, this approach uses state estimation techniques to compensate all those errors and to obtain correct angular rates in real time. The mechanical structure errors discussed in this paper may come from structure designs and fabrication imperfections. The interface circuit errors include: mismatch of differential capacitors, parasitic capacitance, offset voltage of operation amplifiers, and circuit noise. Simulation results indicates that, with the presence of those errors and a signal-to-noise ratio around 20, the proposed method can measure time-varying angular rates with a bandwidth up to 30 Hz and a sensing accuracy of 1×10^{-2} rad/sec. *Copyright © 2009 IFSA.*

Keywords: Interface circuit errors, State observers, Gyroscopes, Extended Kalman filter, Signal drifts

1. Introduction

MEMS vibratory gyroscopes have received lots of attention due to their small size, low cost, integrated circuit (IC) compatibility, and acceptable performance for lots of applications [1]. Conceptually, they act like a proof mass suspended in a rigid frame, as shown in Fig. 1. The mass is driven to vibrate along the "Drive" axis. If the frame rotates along z-axis, a Coriolis force is generated along the "Sense" axis. The angular rate can be obtained by measuring the motions of the proof mass along the "Sense" axis. To this aim, a MEMS vibratory gyroscope consists of three subsystems, as shown in Fig. 2. The "Mechanical structure" converts the Coriolis force into displacements along designated directions. These displacements are then converted into another physical quantity for the ease of measurements (e.g., capacitance variations, resistance variation, etc.). The "Interface circuits" converts these measurements into voltage signals for subsequent signal processing. The "Control algorithm" processes these signals for the feedback control of the proof mass trajectory and for calculating the angular rates. The imperfections existed in each subsystem would significantly degrade the sensing accuracy of angular rates. Even worse, the trend towards miniaturization and better performance decreases the tolerance of imperfections.

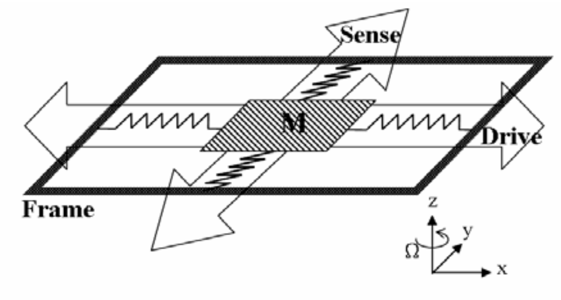

Fig. 1. A schematic of a vibratory gyroscope.

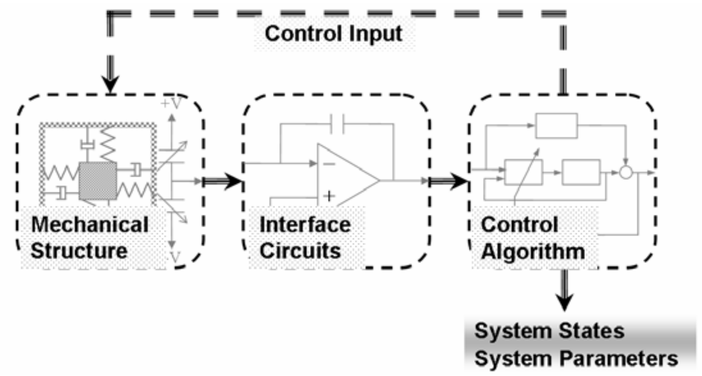

Fig. 2. Block diagram of a vibratory MEMS gyroscope system.

The mechanical structure imperfections mainly come from the structure designs and fabrication errors. For the structure design, it is difficult to design in single-axis resilient forces and small damping forces with MEMS fabrication processes. For the fabrication error, it is normal to have 10 %~20 % dimension variations and residual film stress from process steps such as lithography, etching, film deposition, and etc [2, 3]. All these errors cause the fabricated gyroscope dynamics (spring constants and damping coefficients) deviated from their designated values. Even worse, they induce cross-axis resilient force and cross-axis damping force, which lead to the serious "quadrature error" in gyroscope systems [2]. According to paper survey, solutions to mechanical structure imperfections include: advanced micromachining processes [4, 5], complicated mechanical structure designs [6-8], post-micromachining [9, 10], and etc. In a word, these imperfections are often minimized by expensive tooling processes.

The reactance sensing scheme is attractive to MEMS devices because it can be fairly accurate. Besides, neither additional processing steps nor materials are required for the fabrication process. When adapting this sensing technique, charge amplifiers are often used as an interface circuit to convert capacitance variations into voltage signals [11]. The imperfections in this circuit includes: offset voltage of operational amplifiers, parasitic capacitances, circuit noises, bias ambiguity, and etc. [12]. Several methods have been proposed to deal with those problems including: auto-zeroing, chopper stabilizations, switched capacitor, correlated double sampling, dynamic element matching, and etc. [11-16]. Those approaches are effective and have been widely used. However, they are complicated in circuit designs and may introduce other problems [11, 14-16]. For example, the "switched capacitor" method solved the offset voltage and parasitic capacitance problems, but generated extra noises during capacitor switching [11, 14]. In literatures, we found some papers using control algorithms to compensate imperfections in power IC circuits [17, 18]. However, we have not found one for charge amplifiers, except our preliminary work [19].

Currently, a vibratory gyroscope needs feedback controls to regulate its proof mass trajectory and to obtain angular rates. Among various control algorithms, the parameter estimation method is getting popular because it can achieve above tasks when the mechanical structures are imperfect [20-23]. This method improves the performance of MEMS gyroscopes without expensive tooling processes thus could be promising for the mass production. Unfortunately, in those reports, the interface circuits were all assumed to be ideal.

To sum up, in most existing MEMS systems, the imperfections from mechanical structures and interface circuits were minimized physically and individually. The disadvantage of that is costly. Different from those approaches, this paper presents a control algorithm to compensate imperfections from both mechanical structures and interface circuits for vibratory gyroscopes, and to estimate angular rates in real item. The control algorithm was developed based on the state estimation techniques. The estimation properties and system stability are discussed in details in this paper.

This paper is organized as follows: both the mechanical structure and interface circuit of a gyroscope system are modeled in details and shown in Section 2. The design of a state observer and a feedback controller that can compensate the effect of imperfections are presented in Section 3, followed by their stability analysis shown in Section 4. Several simulation results are shown in Section 5 to verify the analysis discussed previously. Finally, in Section 6 and 7, the paper is concluded and the results are briefly discussed.

2. System Modeling

2.1. Gyroscope Dynamics

A linear vibratory gyroscope can be modeled as a spring-mass-damper system. Assuming that motions of the proof mass are constrained in the x-y plane and the rotation motions of the proof mass are ignored, the dynamics of a gyroscope can be modeled as follows:

$$\begin{aligned} m\ddot{x} + d_{xx}\dot{x} + d_{xy}\dot{y} + k_{xx}x + k_{xy}y &= u_x + 2m\Omega_z\dot{y} \\ m\ddot{y} + d_{xy}\dot{x} + d_{yy}\dot{y} + k_{xy}x + k_{yy}y &= u_y - 2m\Omega_z\dot{x}, \end{aligned} \tag{1}$$

where m is the mass of the proof mass; d_{xx}, d_{yy}, k_{xx}, k_{yy} are damping coefficients and spring constants along two axes x and y; Ω_z is the angular rate to be measured along z-axis; d_{xy} and k_{xy} are the cross-axis damping coefficient and spring constant; u_x and u_y are the control inputs along x and y axis. In most cases, the mass m in (1) is assumed to be known and above equation is normalized to obtain (2).

$$\begin{aligned} \ddot{x} + d_{xx}\dot{x} + d_{xy}\dot{y} + k_{xx}x + k_{xy}y &= u_x + 2\Omega_z\dot{y} \\ \ddot{y} + d_{xy}\dot{x} + d_{yy}\dot{y} + k_{xy}x + k_{yy}y &= u_y - 2\Omega_z\dot{x}, \end{aligned} \tag{2}$$

where $d_{xx} \leftarrow d_{xx}/m$, $d_{xy} \leftarrow d_{xy}/m$, $d_{yy} \leftarrow d_{yy}/m$, $k_{xx} \leftarrow k_{xx}/m$, $k_{xy} \leftarrow k_{xy}/m$, $k_{yy} \leftarrow k_{yy}/m$, $u_x \leftarrow u_x/m$, $u_y \leftarrow u_y/m$. The mechanical structure imperfections would result in the existence of d_{xy}, k_{xy}, and uncertain values of all spring constants and damping coefficients.

2.2. Capacitive Position Sensing

Depending on the mechanism of its varying capacitance design, the capacitive position sensing can be divided into the comb drive scheme and parallel plate scheme [11]. Without losing generality, the comb drive scheme is used to illustrate the concepts here.

As shown in Fig. 3, C_{o1} and C_{o2} are the capacitances when the proof mass is at its nominal position; ΔC_1 and ΔC_2 are the capacitance variations induced by the displacement of the proof mass. A differential capacitor pair design normally requests that C_{o1} equals to C_{o2}; ΔC_1 equals to ΔC_2. However, due to fabrication imperfections, these requirements may not be met. For example, if the nominal position is shifted by a distance d from the neutral position of the structure, the above capacitances can be calculated as follows,

$$
\begin{aligned}
C_{o1} &= N\varepsilon \frac{W}{Z}(x_0 + d) \\
C_{o2} &= N\varepsilon \frac{W}{Z}(x_0 - d) \\
\Delta C_1 &= \Delta C_2 = N\varepsilon \frac{W}{Z} x,
\end{aligned}
\tag{3}
$$

where N is the number of comb fingers; ε is the permittivity of air; W and Z are the height and gap of comb fingers; x_0 is the overlapped length of comb fingers when the proof mass is at its neutral position.

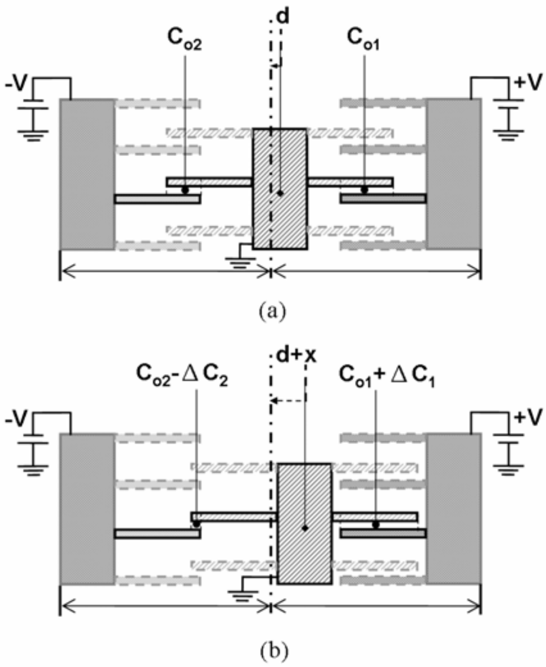

Fig. 3. Comb drive design for the lateral position sensing: (a) the nominal position is shifted by a distance *d*; (b) capacitance variation due to a displacement *x*.

2.3. Interface Circuits

As discussed previously, charge amplifiers are used to convert capacitance variations into voltage signals. And mostly because of the offset voltage of the operational amplifier, modulation techniques are often used to work with the amplifier [12, 14]. Here, the charge amplifier with/without modulation techniques are both analyzed for possible circuit errors.

2.3.1. A Basic Charge Amplifier Circuit

Differential capacitor pair, from the capacitive position sensing design, and a charge amplifier is shown in Fig. 4. C_P is the parasitic capacitance; V_{os} is the offset voltage of the operation amplifier; V_n is the circuit noise.

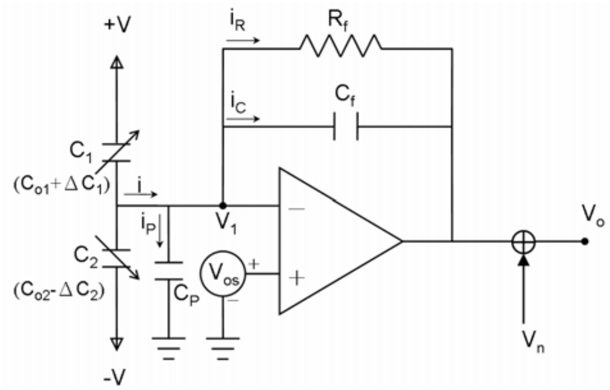

Fig. 4. A schematic of a differential capacitance sensing and a charge amplifier.

When the capacitance variation is induced, charges Q are squeezed out of differential capacitors and flow into R_f, C_f, and C_P. Assuming the differential capacitor pair is biased at constant voltages $\pm V$ and the voltage at the inverting terminal of the operational amplifier is V_1, the charges Q can be calculated as follows:

$$Q = C_1(V - V_1) + C_2(-V - V_1). \tag{4}$$

Assuming no input bias current for the operation amplifier (which is pretty much true for amplifiers made of MOS technology), the current flowing into C_f (i_C) is obtained as:

$$\begin{aligned} i_C &= i - i_P - i_R \\ &= \frac{d(Q)}{dt} - C_P \frac{d(V_1 - 0)}{dt} - \frac{V_1 - V_o}{R_f}. \end{aligned} \tag{5}$$

R_f is often chosen to be large so that it would not destruct the charge sensing [11]; meaning that i_R is negligible. Consequently, the output voltage V_o can be obtained as:

$$
\begin{aligned}
V_o &= -\frac{1}{C_f}\int_0^t i_C\, d\tau + V_1 + V_n \\
&= -(\Delta C_1 + \Delta C_2 + C_{o1} - C_{o2})\frac{V}{C_f} \\
&\quad + (C_{o1} + C_{o2} + \Delta C_1 - \Delta C_2 + C_P + C_f)\frac{V_1}{C_f} + V_n .
\end{aligned}
\tag{6}
$$

If the operational amplifier functions properly in this feedback configuration, V_1 equals to V_{os}. By combining (6) and (3), the output voltage of the interface circuit is:

$$
\begin{aligned}
V_o &= -\frac{2V}{C_f} N\varepsilon \frac{W}{Z} x + \alpha + \beta + V_n \\
\alpha &= \left(2N\varepsilon \frac{W}{Z} d\right)\frac{V}{C_f} \\
\beta &= \left(2N\varepsilon \frac{W}{Z} x_0 + C_P + C_f\right)\frac{V_{os}}{C_f}.
\end{aligned}
\tag{7}
$$

Since the values of d, C_P, and V_{os} are unknown, the values of α and β are unknown. Furthermore, α is an unknown constant; β can either be an unknown constant or a drift depending on whether V_{os} is drifting.

2.3.2. A Charge Amplifier with Modulation Techniques

Fig. 5 shows a schematic of charge amplifier with modulation techniques. The output voltage of this circuit can be calculated as:

$$
\begin{aligned}
V_o &= -(\Delta C_1 + \Delta C_2 + C_{o1} - C_{o2})\frac{V}{C_f} \\
&\quad + \nu(C_{o1} + C_{o2} + \Delta C_1 - \Delta C_2 + C_P + C_f)\frac{V_1}{C_f} + V_{n2} ,
\end{aligned}
\tag{8}
$$

where V_{n2} is the noise at around the modulation frequency and its standard deviation is smaller than that of V_n; ν can be very small depending on the accompanied low-pass filter design. By combining (3) and (8), the output voltage can be rewritten as:

$$
V_o = -\frac{2V}{C_f} N\varepsilon \frac{W}{Z} x + \alpha + \nu\beta + V_{n2}. \tag{9}
$$

From (9) and (7), the output voltages of above two circuits are linearly proportional to the displacement of the proof mass. However, they are both deviated by biases or drifts.

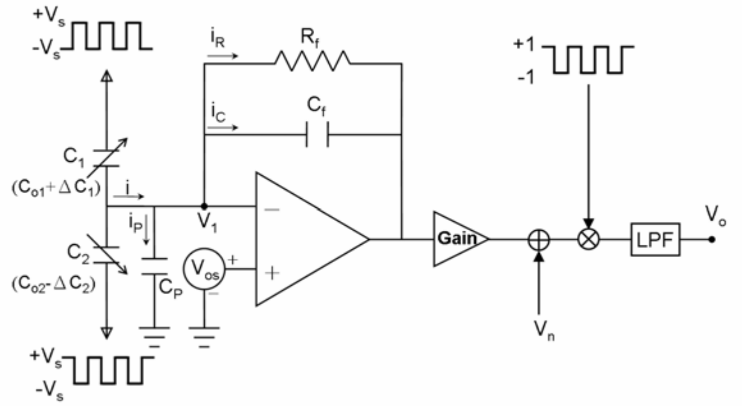

Fig. 5. A schematic of a charge amplifier with modulation techniques.

3. State Observer Design and Feedback Control

To compensate both mechanical structure errors and circuit errors using state estimation techniques, the mechanical structure (2) and interface circuit (7) are modeled together as follows:

$$\begin{aligned}\dot{X} &= f(X) + BU + N_s \\ Z &= HX + N_m,\end{aligned} \tag{10}$$

$$X = \begin{bmatrix} x & \dot{x} & y & \dot{y} & \Phi_x & \Phi_y & \Omega_z & k_{xx} & k_{yy} & k_{xy} & d_{xx} & d_{yy} & d_{xy} \end{bmatrix}^T,$$

$$B = \begin{bmatrix} 0 & 1 & 0 & 0 & [0]_{2\times 9} \\ 0 & 0 & 0 & 1 & \end{bmatrix}^T, \qquad f(X) = \begin{bmatrix} \dot{x} \\ -k_{xx}x - k_{xy}y - d_{xx}\dot{x} - d_{xy}\dot{y} + 2\Omega_z\dot{y} \\ \dot{y} \\ -k_{xy}x - k_{yy}y - d_{xy}\dot{x} - d_{yy}\dot{y} - 2\Omega_z\dot{x} \\ 0 \\ \vdots \\ 0 \end{bmatrix}_{13\times 1},$$

$$H = \begin{bmatrix} \left(-\frac{2V}{C_{fx}} N_x \varepsilon \frac{W_x}{Z_x}\right) & 0 & 0 & 0 & 1 & 0 & [0]_{2\times 7} \\ 0 & 0 & \left(-\frac{2V}{C_{fy}} N_y \varepsilon \frac{W_y}{Z_y}\right) & 0 & 0 & 1 & \end{bmatrix}, \qquad U = \begin{bmatrix} u_x \\ u_y \end{bmatrix},$$

where Z is the output vector of the system; X is the state vector of the system; Φ_x and Φ_y are two bias signals (drifts) at the circuit output. N_m models the noise, while N_s models the Brownian motions of the mechanical structures [24]. Note that Φ_x, Φ_y, Ω_z, spring constants, and damping coefficients are all assumed to be constant for now.

3.1. State Observer Design

With the system equations shown in (10), a state observer can be constructed as follows:

$$\begin{aligned} \dot{\hat{X}} &= f(\hat{X}) + BU + LH(X - \hat{X}) \\ \hat{Z} &= H\hat{X}, \end{aligned} \tag{11}$$

where L is the observer gain and can be chosen from various nonlinear observer algorithms. In this paper, the extended Kalman filtering (EKF) [25] is chosen mainly for its effectiveness in the noise reduction.

When applying EKF to this system, equations (10) are converted into discrete-time difference equations ($\bar{f}$) first. And, the so-called "prediction equations" in the EKF can be calculated by the following steps:

$$\begin{aligned} \hat{X}_{k+1}^{-} &= \bar{f}(k, \hat{X}_k) + BU_k \\ P_k &= E\left[(\hat{X}_k - X_k)(\hat{X}_k - X_k)^T\right] \\ P_{k+1}^{-} &= A_k P_k A_k^T \\ A_k &= \partial\bar{f} / \partial X\big|_{X=\hat{X}_k}, \end{aligned} \tag{12}$$

where the subscript k denotes the value obtained at the $k-th$ sampling time. The "correction equations" in the EKF are:

$$\begin{aligned} L_{k+1} &= P_{k+1}^{-} H^T \left(HP_{k+1}^{-} H^T + R_{k+1}\right)^{-1} \\ P_{k+1} &= (I - L_{k+1} H) P_{k+1}^{-} \\ \hat{X}_{k+1} &= \hat{X}_{k+1}^{-} + L_{k+1} \cdot \left[Z_{k+1} - \hat{Z}(k, \hat{X}_{k+1}^{-})\right], \end{aligned} \tag{13}$$

where L_k is the observer gain; R_k is the covariance matrix of the measurement noise.

In the above derivations, all system parameters are assumed to be constant. However, a functional gyroscope needs to measure time-varying angular rates. Also, the bias voltage of amplifiers could be drifting. To cope with these problems, the fading memory technique [25] is adopted to work with the EKF. This is done by introducing a "forgetting factor, λ" into the prediction equations.

$$P_{k+1}^{-} = \lambda_{k+1} A_k P_k A_k^T. \tag{14}$$

The value of λ can be obtained by assigning a number greater than one or by algorithms shown in [25]. Due to the limited space in this paper, the detail calculations of λ are not shown.

3.2. Feedback Control for Gyroscope System

Since all system parameters and dynamics are estimated in real time, the estimated states can be used to implement feedback controls for gyroscopes. Among various controller designs, we choose the one which keeps the total energy transferred between two axes the same [26]. This control method is chosen because it enforces the feedback system to operate at the resonant frequency of the original system. Thus, the control input can be less. To implement this method, the control input is designed as follows:

$$U = \begin{bmatrix} \hat{d}_{xx}\dot{\hat{x}} + \hat{d}_{xy}\dot{\hat{y}} \\ \hat{d}_{xy}\dot{\hat{x}} + \hat{d}_{yy}\dot{\hat{y}} \end{bmatrix}. \tag{15}$$

Once the values of estimated states and parameters converge to correct values, the trajectory of proof mass can be described by the following equations:

$$\begin{aligned}\ddot{x} + k_{xx}x + k_{xy}y &= 2\Omega_z\dot{y}\\ \ddot{y} + k_{xy}x + k_{yy}y &= -2\Omega_z\dot{x}.\end{aligned} \tag{16}$$

In a special case where $k_{xx} = k_{yy} = k$, the analytical solutions of (16) are:

$$\begin{aligned}x(t) &= \left(\frac{\Psi}{2} - \frac{\Omega_z^2\Psi}{\xi}\right)\cos(\omega_1 t) + \left(\frac{\Psi}{2} - \frac{\Omega_z^2\Psi}{\xi}\right)\cos(\omega_2 t)\\ &\quad + \left(\frac{k_{xy}\Omega_z\Psi}{\xi\omega_1}\right)\sin(\omega_1 t) - \left(\frac{k_{xy}\Omega_z\Psi}{\xi\omega_1}\right)\sin(\omega_2 t)\\ y(t) &= \left(\frac{k_{xy}\Psi}{2\xi}\right)\cos(\omega_1 t) - \left(\frac{k_{xy}\Psi}{2\xi}\right)\cos(\omega_2 t)\\ &\quad - \left(\frac{k\Omega_z\Psi}{\xi\omega_1}\right)\sin(\omega_1 t) + \left(\frac{k\Omega_z\Psi}{\xi\omega_1}\right)\sin(\omega_2 t),\end{aligned} \tag{17}$$

$$\begin{aligned}\omega_1 &= \sqrt{k + 2\Omega_z^2 + \sqrt{k_{xy}^2 + 4\Omega_z^2\left(k + \Omega_z^2\right)}}\\ \omega_2 &= \sqrt{k + 2\Omega_z^2 - \sqrt{k_{xy}^2 + 4\Omega_z^2\left(k + \Omega_z^2\right)}}\\ \xi &= \sqrt{k_{xy}^2 + 4\Omega_z^2\left(k + \Omega_z^2\right)},\end{aligned}$$

where Ψ is the vibration amplitude of the proof mass and is determined by initial conditions of the system.

4. Stability Analysis

The proposed feedback control method is essentially a task of stabilizing a nonlinear system, as shown in (10), using estimated system states. According to Vidyasagar [27], the “separation theorem,” which is often discussed for linear systems, can be applied to nonlinear systems to guarantee their local asymptotical stability. Therefore, the stability analysis can be divided into two tasks: one is a stabilizing controller design and the other is a stable observer design. According to (16) and (17), state values are all bounded. Therefore, it is a stabilizing controller design.

The stability analysis of the observer design can be approached by two steps: the observability of the system; the state convergence of the EKF. For the EKF, it is known that its state convergence is not guaranteed [25]. In that case, one may use the iterative Kalman filter (IKF) to achieve both state convergence and noise reduction at the cost of complicated computations [28].

4.1. Observability Analysis

The observability of a system can be examined by the rank of the observability matrix. The observability matrix of a nonlinear system [29] is obtained by the following:

$$W_o \equiv \frac{\partial}{\partial X}\begin{bmatrix} Z & \dot{Z} & \ddot{Z} & \cdots \end{bmatrix} \quad (18)$$

For this feedback control gyroscope system, the observability matrix (W_o) is calculated and has the following format:

$$W_o = \begin{bmatrix} [W_{ss}]_{6\times6} & [0]_{6\times7} \\ [0]_{7\times6} & [W_{kd}]_{7\times7} \end{bmatrix}_{13\times13}. \quad (19)$$

Due to the diagonal form of W_o, W_{ss} is the observability matrix for the gyroscope dynamics (x, $\dot{x}$, y, $\dot{y}$) and bias signals (Φ_x, Φ_y); W_{kd} is for six system parameters and angular rate. After tedious derivations, the above W_{ss} and W_{kd} matrices can be greatly simplified to the following:

$$W_{ss} = \begin{bmatrix} 1 & 0 & 0 & 0 & 0 & 0 \\ 0 & 0 & 1 & 0 & 0 & 0 \\ 0 & 1 & 0 & 0 & 0 & 0 \\ 0 & 0 & 0 & 1 & 0 & 0 \\ 0 & 0 & 0 & 0 & -k_{xx} & -k_{xy} \\ 0 & 0 & 0 & 0 & -k_{xy} & -k_{yy} \end{bmatrix},$$

$$W_{kd} = \begin{bmatrix} 2\ddot{y} & -\dot{x} & 0 & -\dot{y} & -\ddot{x} & 0 & -\ddot{y} \\ -2\ddot{x} & 0 & -\dot{y} & -\dot{x} & 0 & -\ddot{y} & -\ddot{x} \\ 2y^{(3)} & -\ddot{x} & 0 & -\ddot{y} & -x^{(3)} & 0 & -y^{(3)} \\ -2x^{(3)} & 0 & -\ddot{y} & -\ddot{x} & 0 & -y^{(3)} & -x^{(3)} \\ 2y^{(4)} & -x^{(3)} & 0 & -y^{(3)} & -x^{(4)} & 0 & -y^{(4)} \\ -2x^{(4)} & 0 & -y^{(3)} & -x^{(3)} & 0 & -y^{(4)} & -x^{(4)} \\ 2y^{(5)} & -x^{(4)} & 0 & -y^{(4)} & -x^{(5)} & 0 & -y^{(5)} \end{bmatrix}. \quad (20)$$

For W_{ss}, as long as $k_{xx} \cdot k_{yy} \neq k_{xy}^2$, its rank is six and thus the associated six states are globally observable. Similarly, it can be shown that the rank of W_{kd} is seven if the oscillation of the proof mass contain more than one frequency. According to (17), as long as $k_{xy} \neq 0$ or $\Omega_z \neq 0$, there exists two frequencies in the proof mass trajectory. Thus, the associated seven states are globally observable.

5. Simulations

The HSPICE simulations and Matlab simulations are performed for the circuits shown in Fig. 4 and Fig. 5. In those simulations, the differential capacitors are assumed to be biased at 20 fF. The offset voltage of the amplifier drifts between 0 and 20 mV. The circuit noises consist of white noise and $1/f$ noise. The standard deviation of white noise is 10 mV, and the low-frequency magnitude of the $1/f$ noise is around 50 mV. Other parameters of the circuit are listed in Table 1. As shown at the bottom left of Fig. 6, without modulation techniques, the output of the charge amplifier deviates from their correct values by slow varying drifts and noises. The standard deviation of the noise is calculated to be 15.6 mV. With the modulation technique, shown at the bottom right of Fig. 6, the output signal is bias at 15.5 mV and the standard deviation of the noise is 0.4 mV. The modulation technique reduces the bias values while introducing extra phase lag to the system, which could be a concern for system stability. Both circuits show bias signals (drifts) at their output voltages.

Table 1. Parameters used for the circuit (Figs. 4, 5) simulations.

Parameters	Values
V	1 volt. (DC or 500 kHz)
C_{o1}	220 fF
C_{o2}	180 fF
ΔC	50 fF, 10 kHz
C_P	1 pF
C_f	2 pF
V_{os}	(0 mV to 20 mV)

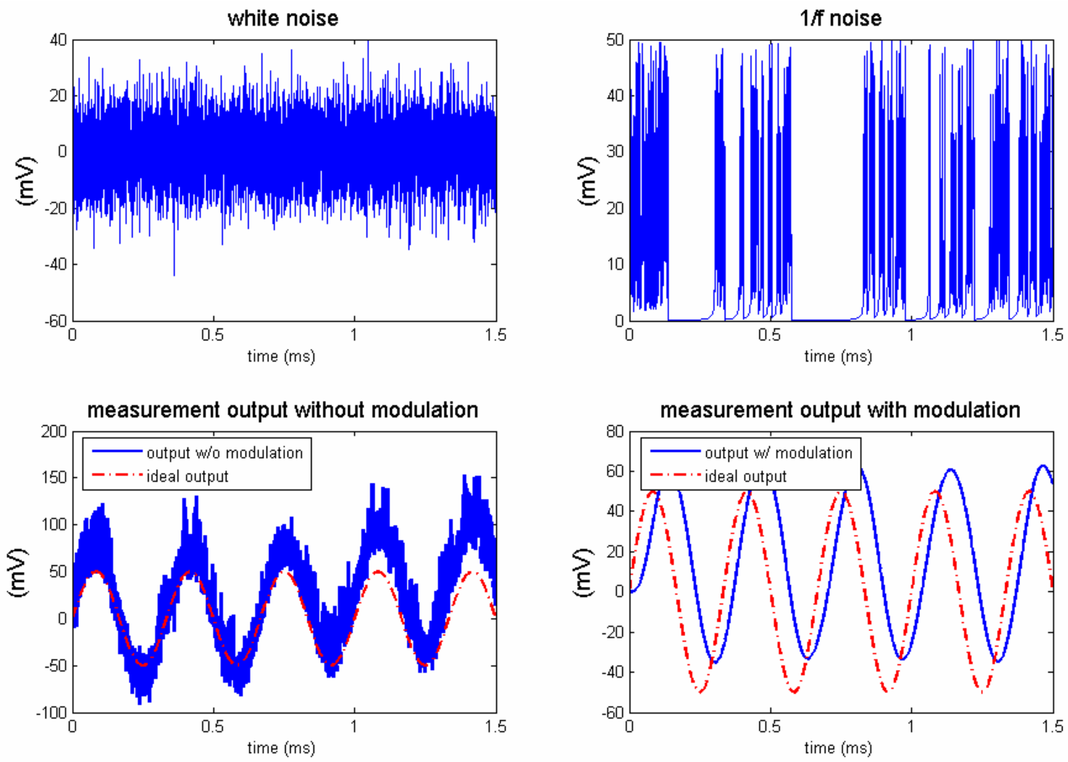

Fig. 6. Voltage outputs of charge amplifiers when there exists mismatched differential capacitors, parasitic capacitance, offset voltages of amplifiers, white noise, and 1/f noise.

In the simulations of gyroscope systems, the proof mass is assumed to be actuated 2 μm at 3 kHz. The angular rate to be measured is 1 rad/sec. The biases of the circuit outputs (Φ_x and Φ_y) are assumed to be 10 mV and 12 mV. The noises that contaminate the circuit output are assumed to be white with a standard deviation of 1 mV. All the system parameters in (1) are assumed to be unknown except the mass of the proof mass. The initial guess of system states in (10) are 15 % to 20 % off from their respective correct values. The correct values of system parameters, normalized by the mass of the proof mass and a characteristic length (2 μm), are listed in Table 2. The sampling rate of the control algorithm is 2.5 MHz. Fig. 7 shows the circuit output of the gyroscope system, which measures the position of the proof mass along x-axis and y-axis.

Table 2. Parameters of the gyroscope system.

Parameters	Values (normalized)
Ω_z	1 rad/sec
k_{xx}	$(2\pi \times 3000)^2 s^{-2}$
k_{yy}	$(2\pi \times 3000)^2 s^{-2}$
k_{xy}	$(2\pi \times 500)^2 s^{-2}$
d_{xx}	10 s^{-1}
d_{yy}	10 s^{-1}
d_{xy}	2 s^{-1}
Φ_x	10 mV
Φ_y	12 mV

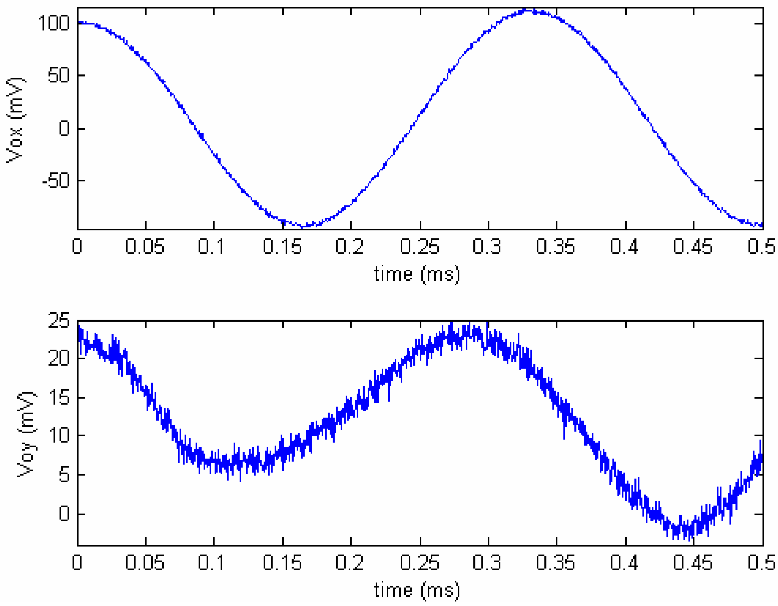

Fig. 7. Circuits outputs for the x-axis (upper) and y-axis (lower) position sensing. The bias signals are 10 mV and 12 mV, respectively. The circuit noises of both axes are white with a standard deviation of 1 mV.

Fig. 8 shows the estimation of the proof mass dynamics using proposed method. According to simulation results, the estimated values quickly converge to their correct values. Fig. 9 shows the estimated values for two bias signals, six system parameters and one angular rate. The estimated values converge to their correct values at around 20 ms. The relative accuracy (defined by (*correct values* - *estimated values*) / *correct values*) of (Φ_x, Φ_y, Ω_z, k_{xx}, k_{yy}, k_{xy}, d_{xx}, d_{yy}, d_{xy}), calculated after 30 ms, are (1.5×10^{-4}, 2.1×10^{-4}, 2.6×10^{-3}, 6.2×10^{-6}, 8×10^{-7}, 2.8×10^{-5}, 2.8×10^{-3}, 3.1×10^{-3}, 1.4×10^{-3}).

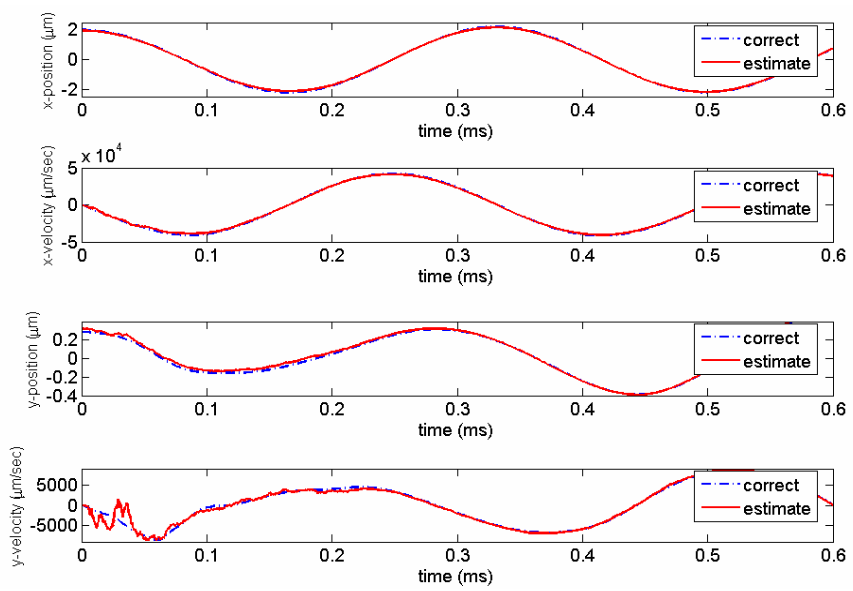

Fig. 8. Estimations of the proof mass dynamics (position and velocity). The estimated values and correct values are almost identical.

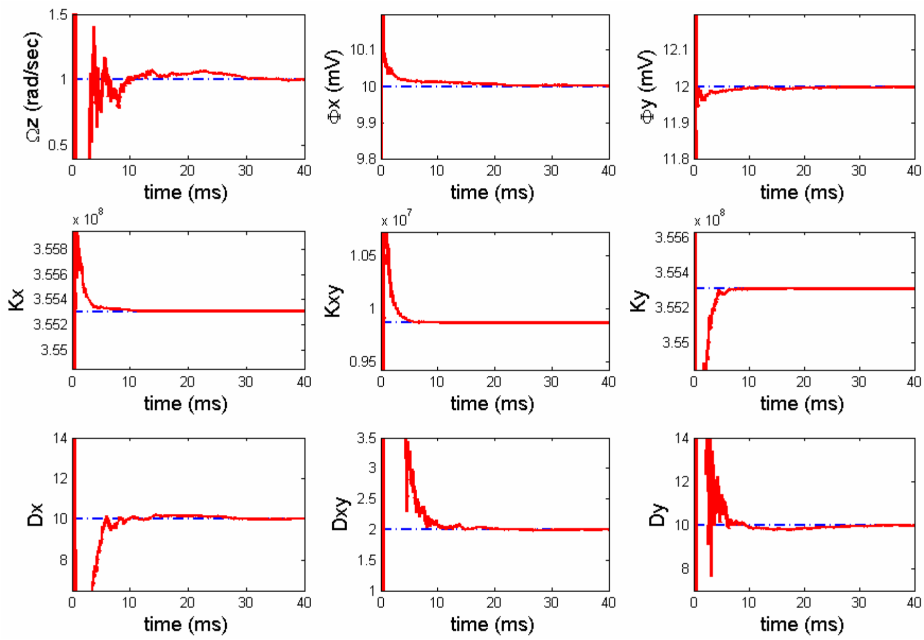

Fig. 9. Estimations of two bias signals, six system parameters, and one angular rate. The estimated values converge to their correct values at around 20 ms.

Fig. 10 shows estimation results when the angular rate and two bias signals are time-varying. The angular rate is 1 $rad/\sec$ at beginning and ramps up with a slope of 15 $rad/\sec^2$ at 36 ms. Similarly, the bias signal Φ_x is 10 mV and ramps up with a slope of 3 mV/sec at 45 ms; Φ_y is 12 mV and ramps up with a slope of 3.5 mV/sec at 45 ms. The fading memory technique is in effect to track time-varying signals while reducing the effect from circuit noise. In this case, the relative accuracy of the following nine states (Φ_x, Φ_y, Ω_z, k_{xx}, k_{yy}, k_{xy}, d_{xx}, d_{yy}, d_{xy}), calculated after 30 ms, are (4.6×10^{-4}, 4.7×10^{-4}, 3.6×10^{-2}, 3.4×10^{-6}, 5.5×10^{-6}, 2.7×10^{-5}, 1.2×10^{-2}, 8×10^{-3}, 9.7×10^{-3}).

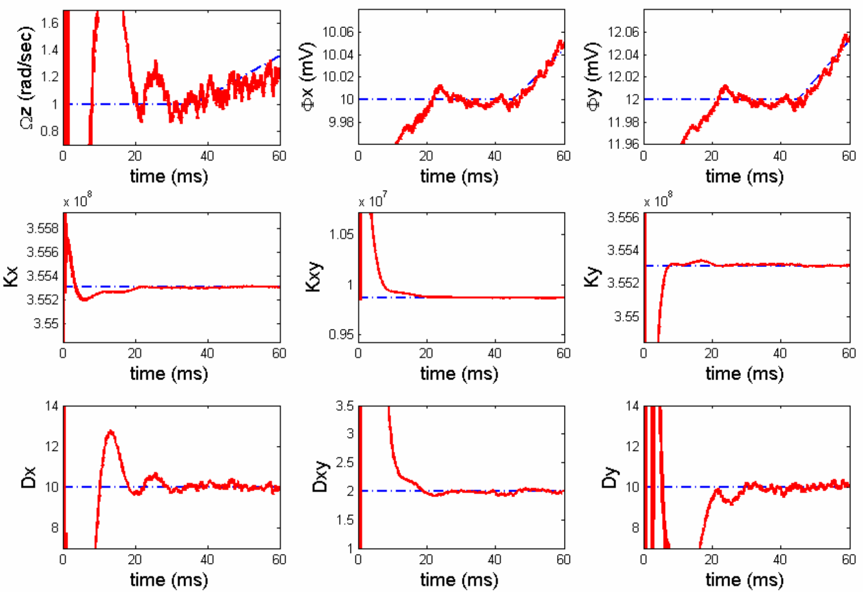

Fig. 10. Estimation of system parameters (states) when the angular rate and two bias signals are time-varying.

Using the proposed method to estimate time-varying angular rates, its frequency response ($\hat{\Omega}_z / \Omega_z$) is shown in Fig. 11. According to the simulation results, the system can measure time-varying angular rates with the frequency of angular rates up to 30 Hz.

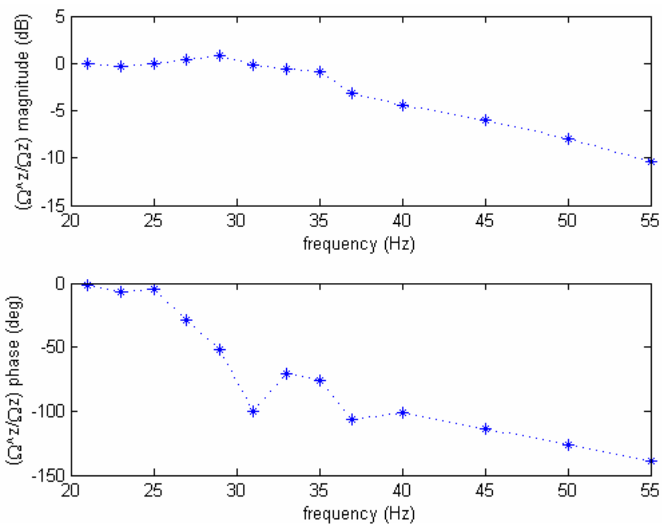

Fig. 11. Frequency response of the proposed gyroscope control system. The system can measure time-varying angular rates with the frequency of angular rates up to 30 Hz.

If system parameters are known and only three parameters (Ω_z, Φ_x, Φ_y) needs to be estimated, the simulation results are shown in the left column of Fig. 12. The estimated values converge to their correct values at around 10 ms, and the relative accuracy are 3.7×10^{-4}, 1.3×10^{-4}, and 4.7×10^{-3}. As compared to the simulation results shown in Fig. 9, the relative accuracy is roughly the same but the converging speed increases, meaning that the system bandwidth could be higher than 30 Hz. Furthermore, as shown in the right column of Fig. 12, the sampling rate of the control algorithms can be lowered to 500 kHz without degrading much of estimation accuracy.

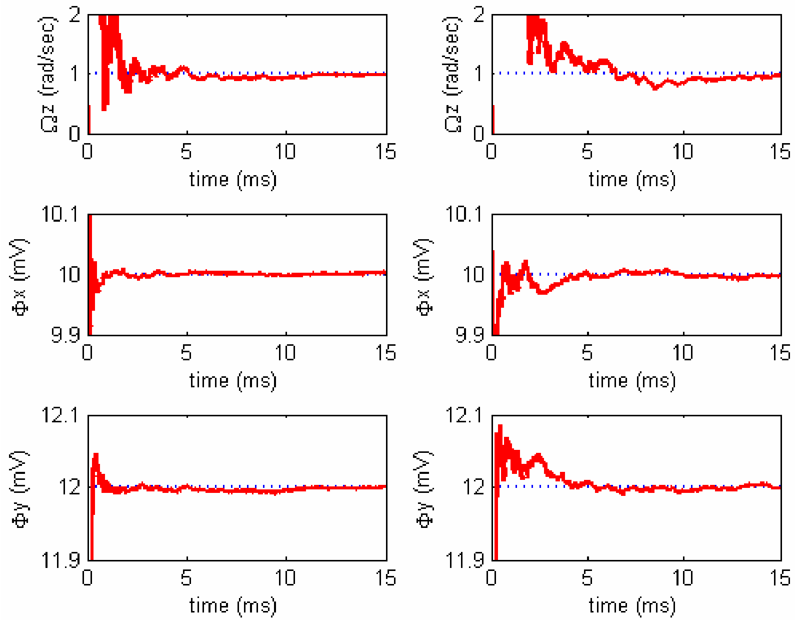

Fig. 12. Parameter estimations when only three unknown parameters in the gyroscope system. The: sampling rate in the left column is 2.5 MHz while it is 500 kHz in the right column.

In order to explore the minimum detectable constant angular rate, we keep lowering the angular rate to be measured until the parameter estimations fail. As shown in Fig. 13, with the existence of both structure uncertainties and signal errors, the minimum detectable angular rate is around 1×10^{-2} rad/sec. Note that, this minimum detectable angular rate is applicable to this special case only.

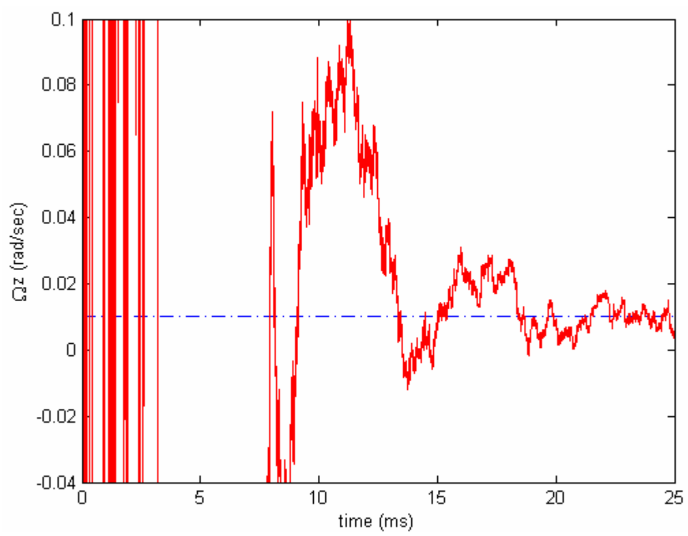

Fig. 13. The minimum detectable angular rate is around 0.01 rad/s when there exists mechanical structure errors, signal drifts and noise.

6. Discussions

The proposed method uses state estimation techniques to compensate circuit imperfections. In essence, these imperfections can be identified is because of the knowledge of accompanied dynamic system. In this case, the signal drifts can be identified because they are not from gyroscopes according to the dynamic equations of gyroscopes. Therefore, the proposed method is not limited to gyroscope systems but can be applied to other feedback control systems that employ the capacitance sensing scheme, such as force-balanced accelerometers [30], microactuators, and etc.

The proposed method uses state estimation to obtain angular rate. Simulation results indicate that the system bandwidth is 30 Hz and the sensing accuracy is 1×10^{-2} rad/sec. For the same gyroscope system using the conventional method (or so called "open loop" control, which assumes the knowledge of all system parameters and perfect sensing circuits [31]), the system bandwidth is around 1 Hz and the sensing accuracy is 7×10^{-2} rad/sec. Comparing to that, the proposed method improves the sensing accuracy by seven times and the response time by 30 times under structure and circuit imperfections.

From the viewpoint of system engineering, the interface circuit imperfections could lead to three possible errors: signal noise, scaling factor error, and signal drift. The proposed method demonstrates its capability in compensating noises and drifts in real time without complicated circuit designs. In this case, the scaling factor error could be induced by the mismatch of capacitance variations ($\Delta C_1 \neq \Delta C_2$). And, our observability analysis indicates that this error can be correctly estimated under certain circumstances. For example, there are two scaling factors in this gyroscope system (position measurements along x-axis and y-axis). And, if one of them is known, the other one can be identified in real time.

7. Conclusions

In this paper, the effect of mechanical structure imperfections were accounted as unknown spring constants and damping coefficients of a dynamic system. The effect of interface circuit imperfections were accounted as unknown signal drifts and measurement noises. The analysis of system observability proves that these unknown parameters can be correctly identified only when the oscillation of the proof mass contains more than one frequency. These parameters were estimated using extended Kalman filter accompanied with fading memory techniques. And, the estimated parameters and estimated system dynamics (velocities and positions) were used to control the proof mass trajectory to meet that frequency requirement and to obtain angular rates in real time.

Simulation results indicate that, with a signal-to-noise ratio around 20, the proposed method can correctly estimate nine parameters with relative accuracies smaller than 10^{-2}. Furthermore, it can measure time-varying angular rates with a bandwidth up to 30 Hz and a sensing accuracy of 1.0×10^{-2} rad/sec. As compared to "conventional methods", which assumes perfect mechanical structures and perfect sensing circuits, the proposed method improves the sensing accuracy by seven times and the bandwidth by 30 times.

References

[1]. A. M. Shkel, Micromachined gyroscopes: challenges, design solutions, and opportunities, in *Proc. of the 4th IEEE Conference on Sensors*, Irvine, California, Oct. 31st – Nov. 3rd, 2001, pp. 74-85.

[2]. A. M. Shkel, R. T. Howe, and R. Horowitz, Modeling and simulation of micromachined gyroscopes in the presence of imperfection, *Proc. of the International Conference on Modeling and Simulation of Microsystems (MSM 99)*, San Juan, Puerto Rico, U. S. A., Apr. 19th -21st, 1999, pp. 605-608.

[3]. M. S. Weinberg and A. Kourepenis, Error sources in in-plane silicon tuning-fork MEMS gyroscopes, *Journal of Microelectromechanical Systems*, Vol. 15, No. 3, 2006, pp. 479-491.

[4]. B. Choi, S. Park, H. Ko, S. -J. Paik, Y. Park, G. Lim, A. Lee, S. -C. Lee, W. Carr, D. Setiadi, R. Mozulay, and D. Cho, The first sub-deg/hr bias stability, silicon-microfabricated gyroscope, *Proc. of the 13th International*

Conference on Solid-State Sensors, Actuators and Microsystems (Transducers '05), Seoul, Korea, Jun. 5th -9th, 2005, pp. 180-183.
[5]. H. Kawai, K. -I. Atsuchi, M. Tamura, and K. Ohwada, High-resolution microgyroscope using vibratory motion adjustment technology, *Sensors and Actuators A: Physical*, 90, 2001, pp. 153-159.
[6]. C. Acar and A. M. Shkel, An approach for increasing drive-mode bandwidth of MEMS vibratory gyroscopes, *Journal of Microelectromechanical Systems*, Vol. 14, No. 3, 2005, pp. 520-528.
[7]. S. E. Alper and T. Akin, A symmetric surface micromachined gyroscope with decoupled oscillation modes, *Sensors and Actuators A: Physical*, 97-98, 2002, pp. 347-358.
[8]. A. S. Phani, A. A. Seshia, M. Palaniapan, R. T. Howe, and J. A. Yasaitis, Modal coupling in micromechanical vibratory rate gyroscopes, *IEEE Sensors Journal*, Vol. 6, No. 5, 2006, pp. 1144-1152.
[9]. M. Ono, N. Wakatsuki, and Y. Takahashi, LiTaO3 single-crystal tuning fork gyroscope, *Electronics and Communications in Japan*, Part Ⅱ, 82, 6, 1999, pp. 82-90.
[10]. S. Gunthner, M. Egretzberger, A. Kugi, K. Kapser, B. Hartmann, U. Schmid, and H. Seidel, Compensation of parasitic effects for a silicon tuning fork gyroscope, *IEEE Sensors Journal*, Vol. 6, No. 3, 2006, pp. 596-604.
[11]. N. Wongkomet, Position sensing for electrostatic micropositioners, *Ph. D. thesis*, *University of California at Berkeley*, 1998.
[12]. C. C. Enz and G. C. Temes, Circuit techniques for reducing the effects of op-amp imperfections: auto-zeroing, correlated double sampling, and chopper stabilization, *Proceedings of the IEEE*, Vol. 84, Issue 11, 1996, pp. 1584-1614.
[13]. B. E. Boser, Electronics for micromachined inertial sensors, in *Proc. of the 9th International Conference on Solid-State Sensors, Actuators and Microsystems (Transducers '97)*, Chicago, U. S. A., Jun. 16th -19th, 1997, pp. 1169-1172.
[14]. A. Bakker, K. Thiele, and J. H. Huijsing, A CMOS nested-chopper instrumentation amplifier with 100-nV offset, *IEEE Journal of Solid-State Circuits*, Vol. 35, No. 12, 2000, pp. 1877-1883.
[15]. M. Tavakoli and R. Sarpeshkar, An offset-canceling low-noise lock-in architecture for capacitive sensing, *IEEE Journal of Solid-State Circuits*, Vol. 38, No. 2, 2003, pp. 244-253.
[16]. Z. Wang, Z. Li, X. Ni, and B. Mo, Electronics for micromachined inertial sensors, in *Proc. of the 8th International Conference on Solid-State and Integrated Circuit Technology (ICSICT '06)*, Shanghai, China, Oct. 23rd -26th, 2006, pp. 673-675.
[17]. Y. -C. Chang and C. -M. Liaw, On the design of power circuit and control scheme for switched reluctance generator, *IEEE Transactions on Power Electronics*, Vol. 23, No. 1, 2008, pp. 445-454.
[18]. K. Liu and M. Stiebler, Voltage control of a switched reluctance generator by means of fuzzy logic approach, in *Proc. of the 6th International Conference on Optimization of Electrical and Electronic Equipments (OPTIM'98)*, Brasov, May 14th-15th, 1998, pp. 443-446.
[19]. C. -Y. Chi, Y. -P. Peng, and T. -L. Chen, Compensation of interface circuit errors for MEMS gyroscopes using state observers, in *Proc. of the 3rd International Conference on Sensing Technology (ICST 2008)*, Taiwan,
Nov. 30th – Dec. 3rd, 2008, pp. 25-30.
[20]. Y. C. Wang, S. G. Adams, J. S. Thorp, N. C. MacDonald, P. Hartwell, and F. Bertsch, Chaos in MEMS, parameter estimation and its potential application, *IEEE Transactions on Circuits and Systems: Fundamental Theory and Applications*, Vol. 45, No. 10, 1998, pp. 1013-1020.
[21]. S. Park and R. Horowitz, New adaptive mode of operation for MEMS gyroscopes, *Journal of Dynamic Systems, Measurement, and Control*, Vol. 126, 2004, pp. 800-810.
[22]. R. P. Leland, Adaptive control of a MEMS gyroscope using Lyapunov methods, *IEEE Transactions on Control Systems Technology*, Vol. 14, No. 2, 2006, pp. 278-283.
[23]. L. Dong and R. P. Leland, The adaptive control system of a MEMS gyroscope with time-varying rotation rate, *American Control Conference (ACC)*, Portland, U. S. A., Jun. 8th -10th, 2005, pp. 3592-3597.
[24]. T. B. Gabrielson, Mechanical-thermal noise in micromachined acoustic and vibration sensors, *IEEE Transactions on Electron Devices*, Vol. 40, No. 5, 1993, pp. 903-909.
[25]. Y. Bar-Shalom, X. R. Li, and T. Kirubarajan, Estimation with applications to tracking and navigation, *John Wiley & Sons*, 2003.
[26]. A. M. Shkel, R. Horowitz, A. A. Seshia, S. Park, and R. T. Howe, Dynamics and control of micromachined gyroscopes, *American Control Conference (ACC)*, San Diego, U. S. A., Jun. 2nd -4th, 1999, pp. 2119-2124.
[27]. M. Vidyasagar, On the stabilization of nonlinear systems using state detection, *IEEE Transactions on Automatic Control*, Vol. AC-25, No. 3, 1980, pp. 504-509.
[28]. B. M. Bell and F. W. Cathey, The iterated Kalman filter update as a Gauss-Newton method, *IEEE Transactions on Automatic Control*, Vol. 38, No. 2, 1993, pp. 294-297.

[29].M. Vidyasagar, Nonlinear Systems Analysis, *Prentice Hall*, 1993.
[30].K. H. -L. Chau, S. R. Lewis, Y. Zhao, R. T. Howe, S. F. Bart, and R. G. Marcheselli, An integrated force-balanced capacitive accelerometer for low-g applications, *Sensors and Actuators A: Physical*, 54, 1996, pp. 472-476.
[31].S. Park, Adaptive Control Strategies for MEMS Gyroscopes, *Ph. D. thesis*, University of California at Berkeley, 2000.

Guide for Contributors

Aims and Scope

Sensors & Transducers Journal (ISSN 1726-5479) provides an advanced forum for the science and technology of physical, chemical sensors and biosensors. It publishes state-of-the-art reviews, regular research and application specific papers, short notes, letters to Editor and sensors related books reviews as well as academic, practical and commercial information of interest to its readership. Because it is an open access, peer review international journal, papers rapidly published in *Sensors & Transducers Journal* will receive a very high publicity. The journal is published monthly as twelve issues per annual by International Frequency Association (IFSA). In additional, some special sponsored and conference issues published annually. *Sensors & Transducers Journal* is indexed and abstracted very quickly by Chemical Abstracts, IndexCopernicus Journals Master List, Open J-Gate, Google Scholar, etc.

Topics Covered

Contributions are invited on all aspects of research, development and application of the science and technology of sensors, transducers and sensor instrumentations. Topics include, but are not restricted to:

- Physical, chemical and biosensors;
- Digital, frequency, period, duty-cycle, time interval, PWM, pulse number output sensors and transducers;
- Theory, principles, effects, design, standardization and modeling;
- Smart sensors and systems;
- Sensor instrumentation;
- Virtual instruments;
- Sensors interfaces, buses and networks;
- Signal processing;
- Frequency (period, duty-cycle)-to-digital converters, ADC;
- Technologies and materials;
- Nanosensors;
- Microsystems;
- Applications.

Submission of papers

Articles should be written in English. Authors are invited to submit by e-mail editor@sensorsportal.com 8-14 pages article (including abstract, illustrations (color or grayscale), photos and references) in both: MS Word (doc) and Acrobat (pdf) formats. Detailed preparation instructions, paper example and template of manuscript are available from the journal's webpage: http://www.sensorsportal.com/HTML/DIGEST/Submition.htm Authors must follow the instructions strictly when submitting their manuscripts.

Advertising Information

Advertising orders and enquires may be sent to sales@sensorsportal.com Please download also our media kit: http://www.sensorsportal.com/DOWNLOADS/Media_Kit_2009.pdf